

# Journal of Materials Chemistry B

Materials for biology and medicine

Accepted Manuscript

This article can be cited before page numbers have been issued, to do this please use: H. Zhang, S. Bo, K. Zeng, J. Wang, Y. Li, Z. Yang, X. Zhou, S. Chen and Z. Jiang, *J. Mater. Chem. B*, 2020, DOI: 10.1039/D0TB00083C.



This is an Accepted Manuscript, which has been through the Royal Society of Chemistry peer review process and has been accepted for publication.

Accepted Manuscripts are published online shortly after acceptance, before technical editing, formatting and proof reading. Using this free service, authors can make their results available to the community, in citable form, before we publish the edited article. We will replace this Accepted Manuscript with the edited and formatted Advance Article as soon as it is available.

You can find more information about Accepted Manuscripts in the [Information for Authors](#).

Please note that technical editing may introduce minor changes to the text and/or graphics, which may alter content. The journal's standard [Terms & Conditions](#) and the [Ethical guidelines](#) still apply. In no event shall the Royal Society of Chemistry be held responsible for any errors or omissions in this Accepted Manuscript or any consequences arising from the use of any information it contains.

## ARTICLE

**Fluorinated porphyrin-based theranostics for dual imaging and chemo-photodynamic therapy**Received 00th January 20xx,  
Accepted 00th January 20xxHuaibin Zhang<sup>a,b</sup>, Shaowei Bo<sup>a</sup>, Kai Zeng<sup>a</sup>, Jie Wang,<sup>a</sup> Yu Li<sup>b</sup>, Shizhen Chen<sup>b</sup>, Zhigang Yang<sup>a</sup>, Xin Zhou<sup>\*b</sup> and Zhong-Xing Jiang<sup>\*a</sup>

DOI: 10.1039/x0xx00000x

Convenient strategies to transform regular liposome or nano-micelle into multifunctional theranostics would be highly valuable in cancer therapy. Herein, we developed an amphiphilic fluorinated porphyrin dendrimer as a multifunctional “add-on” module which would self-assemble onto liposomal drug delivery systems and conveniently transform the liposome into novel theranostics. Through cancer cells and murine xenograft tumor model assays, the theranostics showed valuable fluorescence/<sup>19</sup>F magnetic resonance dual modal imaging and highly efficient chemo-photodynamic therapy. The modular strategy facilitates the convenient and standardized preparation of multifunctional theranostics.

**Introduction**

The integration of multimodal imaging and multiple therapeutic agents into a theranostics is highly attractive in cancer therapy because it may achieve high therapeutic efficacy through comprehensive tumor-drug image guided combination therapy.<sup>[1]</sup> On the therapy side, combination cancer therapy, treating cancer with multiple therapeutic agents, has been approved in clinic to efficiently eliminate cancer cells through multiple mechanisms and reduce drug resistance.<sup>[2]</sup> In recent years, photodynamic therapy (PDT) has become a promising complement to chemotherapy because of its non-invasiveness, low toxicity, repeatability and avoidance of multi-drug resistance.<sup>[3]</sup> On the imaging side, theranostics with multimodal imaging takes the advantages of each imaging technology and provides comprehensive multi-dimensional drug-tumor-therapy images for accurate cancer diagnosis and therapy.<sup>[1]</sup> Among the various imaging modalities, the combination of fluorescence imaging (FL) and <sup>19</sup>F magnetic resonance imaging (<sup>19</sup>F MRI) is highly valuable.<sup>[4]</sup> FL provides high intensity and real-time images in a convenient and well established way, but it suffers the poor penetration of light in deep tissues. While, <sup>19</sup>F MRI complements FL

by providing “hot spot” images without background signal, ionizing radiation, and tissue depth limit.<sup>[5]</sup> Therefore, it would be highly beneficial for cancer therapy to incorporate chemotherapy, PDT, FL, and <sup>19</sup>F MRI into novel theranostics.

However, it would be very challenging to develop such theranostics. First, the relatively low sensitivity of <sup>19</sup>F MRI requires a number of <sup>19</sup>F with similar chemical shifts to achieve high local <sup>19</sup>F concentration,<sup>[4,6]</sup> which would lead to the difficulties in the synthesis of <sup>19</sup>F MRI agents. Second, the low water solubility and strong aggregation of conventional fluorescent agents, PDT photosensitizers and <sup>19</sup>F MRI agents would result in signal quenches, low therapeutic efficacy, formulation issues, etc.<sup>[4a,5,7]</sup> Third, it is difficult to synchronize the drug delivery, release and PDT processes with imaging technologies due to the off-target and premature drug/photosensitizer release issues. To address these issues, a fluorinated amphiphilic porphyrin dendrimer F-PP with FL, <sup>19</sup>F MRI, and PDT capabilities was herein developed as a multifunctional module for the convenient construction of liposomal theranostics (Figure 1). Besides its multifunction, F-PP may be a convenient “add-on” module for existing drug delivery systems (liposomes, micelles, dendrimers, etc.)<sup>[8]</sup> and transform them into theranostics with multimodal imaging and multiple therapeutic agents by self-assembling onto the nanoparticle surface. F-PP contained 3 structural and functional moieties which were connected through 4 L-lysines: a tetrabenzylporphyrin core as both fluorescent chromophore and PDT photosensitizer, 4 highly fluorinated

<sup>a</sup> Hubei Province Engineering and Technology Research Center for Fluorinated Pharmaceuticals and School of Pharmaceutical Sciences, Wuhan University, Wuhan 430071, China.

<sup>b</sup> State Key Laboratory for Magnetic Resonance and Atomic and Molecular Physics, Wuhan Institute of Physics and Mathematics, Chinese Academy of Sciences, Wuhan 430071, China.

\*E-mail: zxjiang@whu.edu.cn, xinzhou@wipm.ac.cn

Electronic Supplementary Information (ESI) available: [details of any supplementary information available should be included here]. See DOI: 10.1039/x0xx00000x

dendrons with 108 symmetrical  $^{19}\text{F}$  as strong  $^{19}\text{F}$  MRI signal emitters, and 4 highly branched monodisperse polyethylene glycols (M-PEGs) as solubility and biocompatibility enhancers. As a water soluble non-ionic amphiphile, F-PP could on one hand avoid the FL and  $^{19}\text{F}$  MRI signal quenches and improve the PDT efficacy by relieving the strong aggregation of porphyrin and fluorocarbons, and on the other hand easily “add-on” to doxorubicin (DOX) loaded liposomes through self-assembly onto the lipid bilayer.<sup>[9]</sup> In addition, when F-PP was anchored on the nanoparticle surface with its 4 hydrophobic fluorinated dendrons, its 12 M-PEGs would PEGylate the liposomes. In these means, a multifunctional theranostics for imaging-guided cancer therapy would be conveniently prepared.

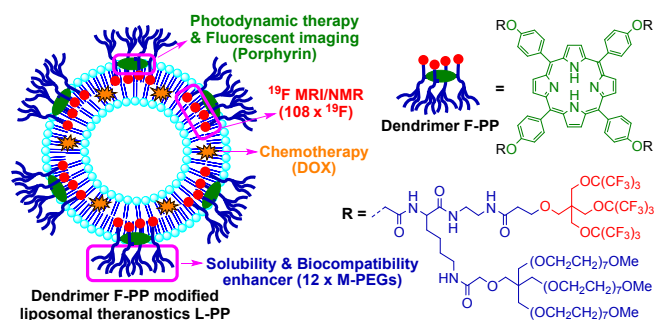


**Figure 1.** Dendrimer F-PP as “add-on” module for theranostics L-PP.

## Experimental

### Cellular uptake of F-PP and L-PP

The cellular uptake of F-PP was detected in HepG2 cells using confocal microscope. Briefly, HepG2 cells were seeded into confocal dishes and incubated at 37 °C for 24 h. Then the medium was removed and replaced with medium of F-PP (5 mg/mL). After 2 h incubation, the medium was removed and washed with PBS buffer, followed by DAPI staining to the nuclei for 5 min, and then to image using confocal microscope. The cellular uptake of DOX and L-PP used the same procedure.

### Detection of singlet oxygen in vitro

HepG2 cells were seeded in a 6-well plate at a density of  $2 \times 10^5$  /mL, and incubated with L-PP (10  $\mu\text{M}$  F-PP) at 37 °C for 2 h. After washing with PBS, the cells were incubated with carboxy- $\text{H}_2\text{DCFDA}$  (25  $\mu\text{M}$ ) for 30 min, then washed again with PBS and irradiated with a 650 nm laser at a power density of 100  $\text{mW}/\text{cm}^2$  for 5 min per well. The cells were fixed with 4% formaldehyde polymer for 10 min and washed with PBS for 3

times. Finally, cells were imaged under Confocal Laser Scanning Microscope (A1R/A1, Nikon, Japan). DOI: 10.1039/D0TB00083C

### In vitro phototoxicity

HepG2 cells were seeded into 96-well plates and incubated for 12 h. The cells were incubated with DOX and L-PP (0, 0.5, 1, 2, 5 and 10  $\mu\text{g}/\text{mL}$  DOX) for 24 h at 37 °C respectively. After washed with PBS, the cells were irradiated with a 650 nm laser at a power density of 100  $\text{mW}/\text{cm}^2$  for 5 min. The non-irradiation group was kept under same conditions except for irradiation. Methylthiazolytetrazolium (MTT) assay kit was employed to evaluate cell toxicity.

To staining of live and dead cells, cells were seeded in a 6-well plate and incubated with L-PP (10  $\mu\text{M}$  F-PP) at 37 °C for 2 h, washed with PBS and irradiated with a 650 nm laser at a power density of 100  $\text{mW}/\text{cm}^2$  for 10 min. then the cells were incubated with calcein AM (4  $\mu\text{M}$ ) and propidium iodide (4  $\mu\text{M}$ ) for 30 min and 5 min respectively. Cellular fluorescence image was obtained by Confocal Laser Scanning Microscope (A1R/A1, Nikon, Japan).

### In vivo $^{19}\text{F}$ MRI experiments

HepG2 tumor bearing Balb/c nude mice were purchased from Cloud-Clone Corp. (CCC, Wuhan) and used for the in vivo evaluation of L-PP. In this study, mice was injected with 250  $\mu\text{L}$  L-PP (42.4  $\mu\text{M}/\text{kg}$  of F-PP) via the tail vein and anesthetized by isoflurane. All animal experimental procedures, including in vivo  $^{19}\text{F}$  MRI experiments, fluorescence imaging, chemotherapy and phototherapy, were performed in accordance with the National Institutes of Health Guide for the Care and Use of Laboratory Animals and were approved by the Institutional Animal Care and Use Committee of Wuhan University.  $^1\text{H}$  MRI: method = RARE, matrix size = 256 $\times$ 256, FOV = 40 mm  $\times$ 30 mm, TR = 2500 ms, TE = 33 ms, RARE factor = 8, number of average = 4, scan time = 80 s;  $^{19}\text{F}$  MRI: method = RARE, Matrix size = 32 $\times$ 32, FOV = 40 mm $\times$ 30 mm, TR = 1600 ms, TE = 2.95 ms, RARE factor = 4, number of average = 64, scan time = 13 min.

### Fluorescence imaging

For in vivo experiments, 250  $\mu\text{L}$  of L-PP (42.4  $\mu\text{M}/\text{kg}$  of F-PP) were intravenously injected into the HepG2 tumor-bearing mice and the fluorescent images were obtained at 4 h, 8 h, 12 h, 24 h, 48 h, respectively. Fluorescence imaging of organs were

obtained from the organs collected from sacrificed mice after the 48 h *in vivo* imaging. The fluorescent scans were recorded on IVIS spectrum system. Fluorescence imaging was performed using a 640 nm excitation and a 720 nm emission filter.

### In vivo chemotherapy and phototherapy

HepG2 tumor bearing Balb/c nude mice were divided into 4 treatment groups: 1) Saline; 2) DOX; 3) L-PP; 4) L-PP + laser. The 4 groups of mice were injected by tail vein on day 0, 3, 6, respectively. The DOX doses for DOX group, L-PP group and L-PP + laser group were 5 mg/kg and the F-PP doses for L-PP group and L-PP + laser group were 3  $\mu\text{M}/\text{kg}$ , respectively. Twelve hours post L-PP injection, the mice in group 4 was irradiated with a 650 nm laser at a power density of 100  $\text{W}/\text{cm}^2$  for 10 min. The body weight and tumor volume of mice were measured every 2 days for a period of 21 days. The tumour volume was calculated according to the following formula:  $\text{volume} = (\text{width}^2 \times \text{length})/2$ .

## Results and discussion

### Synthesis and physicochemical property of F-PP

Dendrimer F-PP was synthesized in a convergent way on gram scales and fully characterized with HPLC,  $^{19}\text{F}/^1\text{H}/^{13}\text{C}$  NMR, and MS (Supporting Information). F-PP gave a singlet  $^{19}\text{F}$  NMR peak at 72.34 ppm from its 108 symmetrical  $^{19}\text{F}$  (Figure 2a), distinctive concentration-dependent UV absorption at 420 nm, 517 nm, 554 nm, 595 nm, and 651 nm (Figure 2b), and fluorescent emission at 660 nm, 725 nm, and 788 nm (Figure 2c). Although it contained highly hydrophobic fluorinated dendrons and tetrabenzylporphyrin, F-PP is freely soluble in water because of its 12 hydrophilic M-PEGs. Notably, F-PP had a low self-aggregation tendency in water because no detectable nanoparticle was found by dynamic light scattering (DLS), which was further confirmed by the solvent-dependent UV absorption, fluorescent emission and  $^{19}\text{F}$  NMR of F-PP (Supporting Information). Such non-aggregative behaviour of fluorinated dendrimer was also reported by Yu et al.<sup>[9]</sup> Because of its excellent solubility and low aggregation tendency in water, the aggregation-induced self-quenching, which is a major issue in porphyrins-based FL and PDT agents, was not observed in F-PP. Importantly, even at high concentrations, F-PP exhibited high biocompatibility toward a series of cell lines, including L02 cells, HepG2 cells and MCF-7 cells

(Figure 2d). Here, the M-PEGs in F-PP played a crucial role in its high biocompatibility.

DOI: 10.1039/D0TB00083C

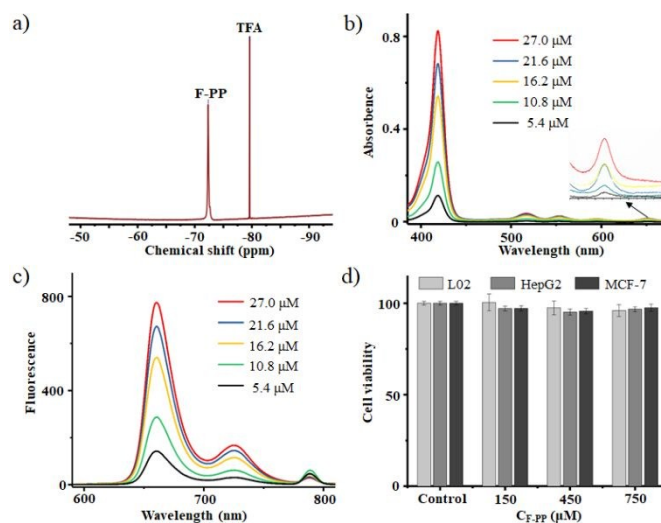


**Figure 2.**  $^{19}\text{F}$  NMR (a, 376 MHz, in water, TFA as internal standard), concentration-dependent UV absorption (b, in water) and fluorescence emission (c, in water), and biocompatibility assay (d) of F-PP.

### In vitro imaging and cell uptake

The designed liposomal theranostics L-PP was formulated through a film dispersion method with both hydrogenated soybean phosphatidylcholine (HSPC) and F-PP as the surfactants, cholesterol as an additive, and DOX as the chemotherapy drug. A DOX encapsulation efficiency of 86% and a DOX loading content of 6% were obtained for L-PP (Supporting Information). DLS of L-PP showed a particle size of 121 nm and a polydispersity index of 0.146 (Figure 3a). L-PP exhibited good stability over 15 days and a pH sensitive drug release profile (Supporting Information). As expected, all the  $^{19}\text{F}$  in L-PP accumulatively gave a strong singlet  $^{19}\text{F}$  NMR peak at 72.61 ppm (Figure 3b) with pretty short  $^{19}\text{F}$  relaxation times (Supporting Information, F-PP:  $T_1 = 375$  ms,  $T_2 = 10$  ms; L-PP:  $T_1 = 439$  ms,  $T_2 = 9$  ms, at 376 MHz), which facilitated 100%  $^{19}\text{F}$  utilization and rapid data collection time for highly sensitive  $^{19}\text{F}$  MRI. A detectable concentration of 99  $\mu\text{M}$  F-PP (or 10.7 mM  $^{19}\text{F}$ ) with a scan time of 160 seconds was achieved for L-PP in  $^{19}\text{F}$  MRI phantom experiments (Figure 3c). It is noteworthy that  $^{19}\text{F}$  MRI signal intensities (SI) of F-PP and L-PP are proportional to their  $^{19}\text{F}$  concentrations, respectively (Figure 3d), which would be valuable for quantifying F-PP and L-PP with  $^{19}\text{F}$  MRI signal intensity. Confocal microscopy images of L-PP treated HepG2 cells indicated that both F-PP and DOX were



efficiently delivered into the cells, especially in the nucleus (Figure 3e). In contrast, F-PP was mainly distributed in the cytoplasm of F-PP treated HepG2 cells (Supporting Information). Notably, the “add-on” of F-PP in L-PP was confirmed by both the  $^{19}\text{F}$  NMR chemical shift change from 72.34 ppm in F-PP to 72.61 ppm in L-PP and no detection of unencapsulated F-PP from Microspin G-50 column treated L-PP.

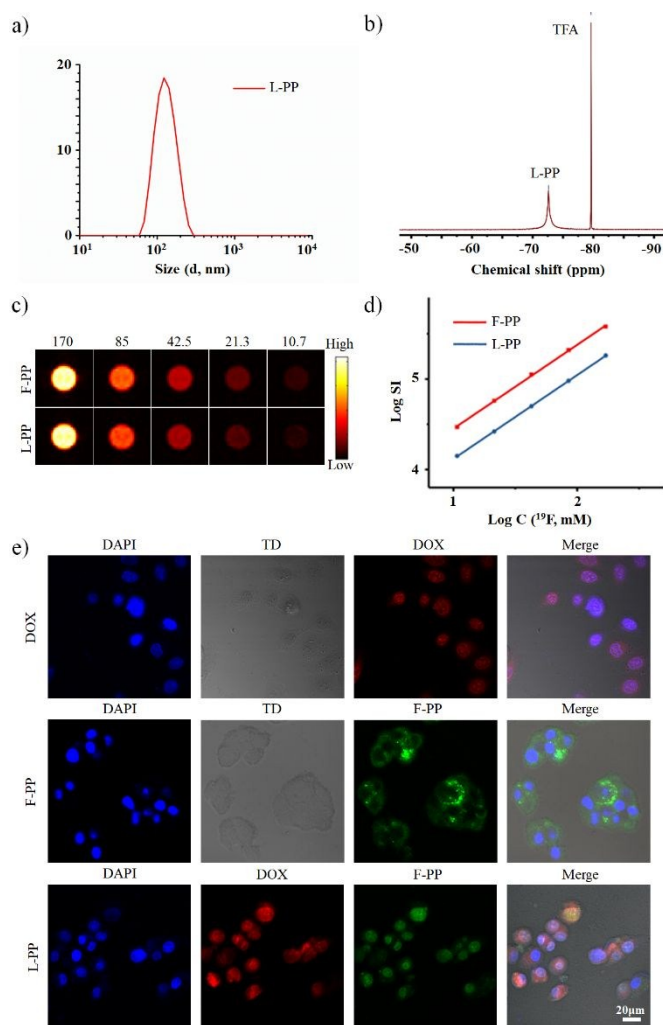


**Figure 3.** DLS (a) and  $^{19}\text{F}$  NMR (b, 376 MHz, in water, TFA as internal standard) of L-PP,  $^{19}\text{F}$  MRI (c, in water) and SI versus  $C(^{19}\text{F})$  plot (d) of L-PP and F-PP, and confocal images of HepG2 cells after 2 h of treatment with DOX, F-PP or L-PP (e).

#### The photodynamic properties of theranostics L-PP

The PDT effect and cytotoxicity of L-PP were investigated in HepG2 cells. First, using a commercial probe 6-carboxy-2',7'-dichlorodihydrofluorescein diacetate ( $\text{H}_2\text{DCFDA}$ ), the reactive oxygen species (ROS) generating ability of L-PP in HepG2 cells was evaluated (Figure 4a). Without L-PP treatment or 650 nm laser

irradiation, neglectable ROS in HepG2 cells was detected by the green fluorescence of  $\text{H}_2\text{DCFDA}$ , while most HepG2 cells with the treatment of L-PP and 650 nm laser irradiation at 100  $\text{mW}/\text{cm}^2$  for 5 min emitted green fluorescence of  $\text{H}_2\text{DCFDA}$ . So, L-PP can significantly improve the oxidative stress of HepG2 cells with a low power density laser irradiation. Second, cytotoxicity assay showed the high combination therapy efficiency of chemotherapy and PDT (Figure 4b). Comparing to DOX, L-PP showed slightly lower cytotoxicity towards HepG2 cells. The cytotoxicity was dramatically improved by the PDT effect when HepG2 cells were treated with both L-PP and low power density laser irradiation. Third, calcein-AM/PI double staining, in which green fluorescent from calcein-AM represented live cells and red fluorescent from PI represented dead or later apoptosis cells, was employed to assess the PDT enhancement efficacy (Figure 4c). After 10 min laser irradiation, most L-PP treated HepG2 cells were killed and emitted red fluorescence, which resulted in a clear border between live and dead cells around the light spot. Therefore, L-PP successfully integrated the chemotherapy of DOX and the PDT of F-PP for enhanced therapeutic efficacy in cancer cells.

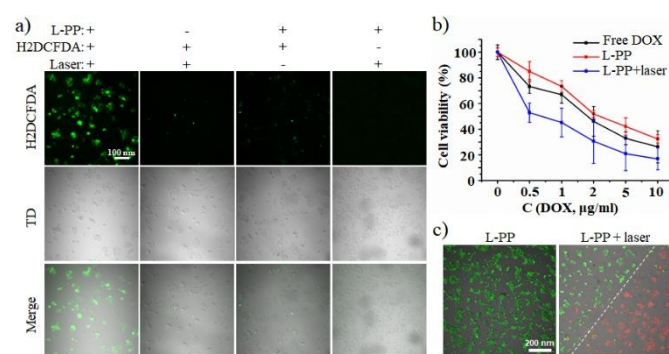


**Figure 4.** Confocal images (a), relative viability (b), and fluorescence images of live/dead cell staining (c) of HepG2 cells after 2 h of treatment with the indicated materials. L-PP in a and c contained 10  $\mu\text{M}$  F-PP. 5 min (a, b) and 10 min (c) of 650 nm laser irradiation at 100  $\text{mW}/\text{cm}^2$  were applied.

#### In vivo fluorescence imaging and $^{19}\text{F}$ MRI of HepG2 tumor

The in vivo FL and  $^{19}\text{F}$  MRI dual imaging of theranostics L-PP was carried out in a xenograft HepG2 liver tumor nude mouse model. First, the biodistribution of L-PP in shallow organs was investigated with FL, which showed the gradually accumulating of L-PP in the tumor region after tail vein injection of L-PP (Figure 5a, a dose of 42  $\mu\text{M}/\text{kg}$  F-PP). Second, the

accumulation of L-PP in tumor was also investigated with  $^{19}\text{F}$  MRI. With a F-PP dose as low as  $42\ \mu\text{M}/\text{kg}$ ,  $^{19}\text{F}$  MRI gave clear "hot spot" images of L-PP in tumor region (Figure 5b, tumor containing cross sections). Comparing to FL,  $^{19}\text{F}$  MRI provided more detailed and accurate images of L-PP in tumor. The accumulation of L-PP in tumor, especially inside of tumor, was clearly showed by  $^{19}\text{F}$  MRI, while FL could hardly show the vivid distribution of L-PP in tumor. Third, the accumulation of L-PP in tumor was quantitatively analysed with the SI of in vivo FL and  $^{19}\text{F}$  MRI. A peak intensity of L-PP in tumor at 24 h post injection was found by both imaging technologies, in which different anesthetics used in the imaging process led to slightly different accumulation profiles (Figure 5c and 6d). Fourth, the biodistribution of L-PP in tumor and internal organs was further studied with ex vivo FL of tumor and organs, which also indicated a high tumor accumulation of L-PP (Figure 5e and 5f). Thus, the two complementary imaging technologies: FL with high sensitivity and  $^{19}\text{F}$  MRI without tissue depth limit, together provided sensitive, accurate, and quantitative in vivo information of L-PP.

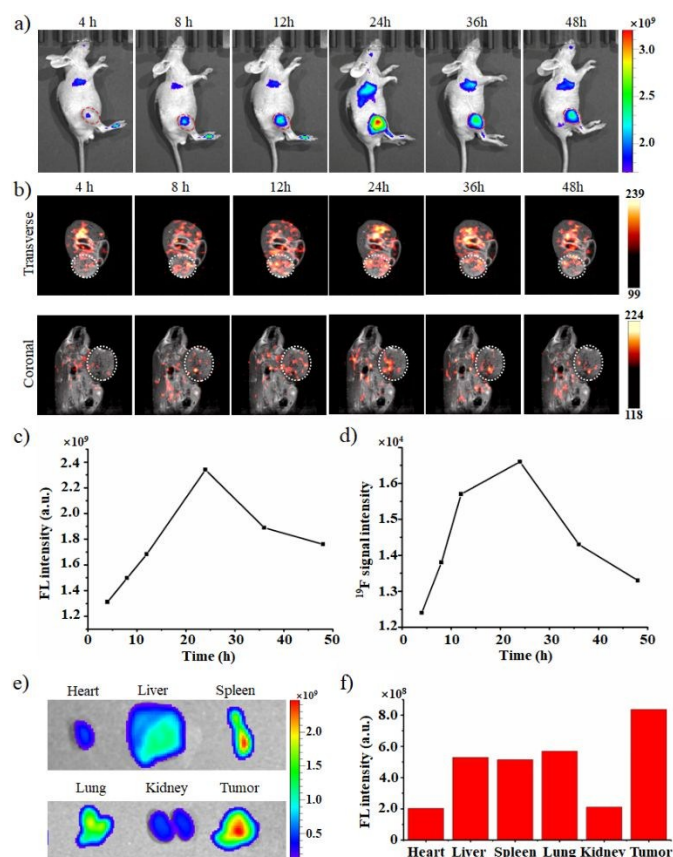


**Figure 5.** In vivo FL (a),  $^{19}\text{F}$  MRI (b, upper: transverse section, lower: coronal section, tumor was marked with a white dot

circle), tumor region SI curves of FL (c) and  $^{19}\text{F}$  MRI (d, transverse section) of mice after intravenous injection of L-PP, ex vivo FL (e) and quantitative SI analysis (f) of major organs and tumor collected from mice sacrificed 48 h post injection.

### Therapy of HepG2 tumor

With the high tumor accumulation of L-PP, the in vivo combination cancer therapy with the DOX-based chemotherapy and F-PP-based PDT of L-PP was investigated in 4 groups of xenograft HepG2 liver tumor mice ( $n = 5$ ). On day 0, 3 and 6, the mice were treated with saline (negative control), DOX (positive control), L-PP, L-PP plus 650 nm laser irradiation at  $100\ \text{mW}/\text{cm}^2$  for 5 min, respectively. First, comparing to chemotherapy with DOX or L-PP, the combination therapy with L-PP plus laser irradiation showed significantly enhanced tumor growth inhibition, in which almost no tumor growth was observed during the study (Figure 6a). Second, due to the toxicity of DOX, the mice in the DOX treatment group showed dramatical body weight loss and all died between day 10 and day 20 (Figure 6b, 6c). Although L-PP showed less tumor growth inhibition capability than DOX, the L-PP treatment groups showed dramatically less body weight loss and full survival rate (Figure 6a-6c). Finally, high therapeutic efficacy and lower systematic toxicity were identified for the combination therapy group because much less toxicity to heart, liver, spleen, lung and kidneys and much higher therapeutic effects in tumor were found by H&E staining of the tissues collected from the mice (Figure 6d and Supporting Information).

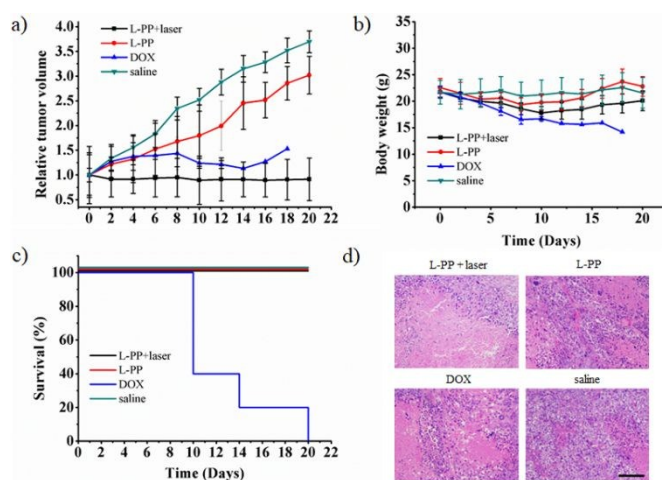


**Figure 6.** Tumor growth curves (a), body weight curves (b), and mice survival curves (c) of HepG2 tumor-bearing nude mice after the indicated group treatments, representative H&E

staining of tumor after group treatments (d). (Data in a and b were expressed as mean  $\pm$  SD, n=5. Scale bar, 100  $\mu$ m.)

## Conclusions

In summary, we have developed a fluorinated porphyrin dendrimer as an “add-on” module for the convenient construction of multifunctional liposomal theranostics for cancer therapy. The “add-on” module showed valuable fluorescent properties, such as high solubility, high fluorescent intensity, no self-aggregation and aggregation-induced signal quenching, and preferred  $^{19}\text{F}$  MRI properties, such as a single  $^{19}\text{F}$  NMR peak, short relaxation times, high  $^{19}\text{F}$  MRI sensitivity. The dual imaging modalities complement each other by provided not only highly sensitive and convenient FL of cells and shallow organs, but also sensitive and quantitative  $^{19}\text{F}$  MRI of deep organs without tissue depth limit. It was found that  $^{19}\text{F}$  MRI provided much more accurate and vivid in vivo images of the drug delivery system in murine. The FL and  $^{19}\text{F}$  MRI dual image-guided combination cancer chemotherapy and PDT have been demonstrated in both cancer cells and murine xenograft tumor model with significantly higher therapeutic efficacy and overall survival of animal. As it would self-assemble onto liposomal drug delivery systems, the fluorinated porphyrin dendrimer may be employed as a general “add-on” modular for various liposomal theranostics, not limited to DOX-load liposomes in this case, and provided them with nanoparticle PEGylation, FL,  $^{19}\text{F}$  MRI, and PDT for image-guided combination therapy. With this modular strategy, many versatile theranostics may be developed in a simplified, standardized, controllable and precise manner for challenging disease therapy.

## Conflicts of interest

The authors have declared that no competing interest exists.

## Acknowledgements

We are thankful for financial support from the National Key R&D Program of China (2016YFC1304704, 2018YFA0704000), the National Natural Science Foundation of China (21572168, 91859206, and 81625011), the Key Research Program of Frontier Sciences, CAS (QZYDY-SSW-SLH018).

## Notes and references

- a) X.-R. Song, S.-X. Yu, S.-H. Li, J. Li, H.-H. Yang, X. Wang, J. Cao, G. Liu, X. Chen, *Adv. Mater.* 2015, **27**, 3285; b) Q. Chen, X. Wang, C. Wang, L. Feng, Y. Li, Z. Liu, *ACS Nano* 2015, **9**, 5223; c) J. Mou, T. Lin, F. Huang, H. Chen, J. Shi, *Biomaterials*, 2016, **84**, 13; d) S. Lu, X. Li, M. Shen, X. Shi, J. Zhang, C. Peng, *Adv. Sci.* 2018, **5**, 1801612; e) B. Yu, H. Wei, Q. He, F. A. Ferreira, C. J. Kuttyreff, D. Ni, Z. T. Rosenkrans, L. Cheng, F. Yu, J. Engle, X. Lan, W. Cai, *Angew. Chem. Int. Ed.* 2018, **57**, 218; f) Y. Li, Y. Wu, J. Chen, J. Wan, C. Xiao, J. Guan, X. Song, S. Li, M. Zhang, H. Cui, T. Li, X. Yang, Z. Li, X. Yang, *Nano Lett.* 2019, **19**, 5806.
- a) M. Saad, O. B. Garbuzenko, T. Minko, *Nanomedicine* 2008, **3**, 761; b) A. Jhaveri, P. Deshpande, V. Torchilin, *J. Control. Release* 2014, **190**, 352; c) G. Shim, M.-G. Kim, D. Kim, J. Y. Park, Y.-K. Oh, *Adv. Drug Delivery Rev.* 2017, **115**, 57; d) S. Shen, M. Liu, T. Li, S. Lin, R. Mo, *Biomater. Sci.* 2017, **5**, 1367; e) S. Gao, G. Tang, D. Hua, R. Xiong, J. Han, S. Jiang, Q. Zhang, C. Huang, *J. Mater. Chem. B* 2019, **7**, 709.
- a) B. M. Luby, C. D. Walsh, G. Zheng, *Angew. Chem. Int. Ed.* 2019, **58**, 2558; *Angew. Chem.* 2019, **131**, 2580; b) S. Mallidi, S. Anbil, A.-L. Bulin, G. Obaid, M. Ichikawa, T. Hasan, *Theranostics* 2016, **6**, 2458; c) X. Li, S. Lee, J. Yoon, *Chem. Soc. Rev.* 2018, **47**, 1174; d) X. Li, N. Kwon, T. Guo, Z. Liu, J. Yoon, *Angew. Chem. Int. Ed.* 2018, **57**, 11522; e) S. Monro, K. L. Colon, H. Yin, J. Roque, P. Konda, S. Gujar, R. P. Thummel, L. Lilge, C. C. Cameron, S. A. McFarland, *Chem. Rev.* 2019, **119**, 797; f) W. Ma, S. Sha, P. Chen, M. Yu, J. Chen, C. Huang, B. Yu, Y. Liu, L. Liu, Z. Yu, *Adv Healthc Mater.* 2020, **9**, 1901100; g) Y. Xiao, F.-F. An, J. Chen, S. Xiong, X.-H. Zhang, *J. Mater. Chem. B* 2018, **6**, 3692.
- a) J. M. Janjic, M. Srinivas, D. K. K. Kadayakkara, E. T. Ahrens, *J. Am. Chem. Soc.* 2008, **130**, 2832; b) S. Mizukami, R. Takikawa, F. Sugihara, M. Shirakawa, K. Kikuchi, *Angew. Chem. Int. Ed.* 2009, **48**, 3641; c) B. E. Rolfe, I. Blakey, O. Squires, H. Peng, N. R. B. Boase, C. Alexander, P. G. Parsons, G. M. Boyle, A. K. Whittaker, K. J. Thurecht, *J. Am. Chem. Soc.* 2014, **136**, 2413; d) S. Bo, C. Song, Y. Li, W. Yu, S. Chen, X. Zhou, Z. Yang, X. Zheng, Z.-X. Jiang, *J. Org. Chem.* 2015, **80**, 6360; e) Y. Zhang, S. Bo, T. Feng, X. Qin, Y. Wan, S. Jiang, C. Li, J. Lin, T. Wang, X. Zhou, Z.-X. Jiang, P. Huang, *Adv. Mater.* 2019, **31**, 1806444; f) J. Zhu, Y. Xiao, H. Zhang, Y. Li, Y. Yuan, Z. Yang, S. Chen, X. Zheng, X. Zhou, Z.-X. Jiang, *Biomacromolecules* 2019, **20**, 1281.
- a) J. Ruiz-Cabello, B. P. Barnett, P. A. Bottomley, J. W. Bulte, *NMR Biomed.* 2011, **24**, 114; b) J. C. Knight, P. G. Edwards, S. J. Paisey, *RSC Adv.* 2011, **1**, 1415; c) I. Tirotta, V. Dichiarante, C. Pigliacelli, G. Cavallo, G. Terraneo, F. B. Bombelli, P. Metrangolo, G. Resnati, *Chem. Rev.* 2015, **115**, 1106.
- a) Z.-X. Jiang, X. Liu, E.-K. Jeong, Y.B. Yu, *Angew. Chem. Int. Ed.* 2009, **48**, 4755; b) S. Temme, C. Grapentin, C. Quast, C. Jacoby, M. Grandoch, Z. Ding, C. Owenier, F. Mayenfels, J. W. Fischer, R. Schubert, *Circulation* 2015, **131**, 1405; c) W. Yu, Y. Yang, S. Bo, Y. Li, S. Chen, Z. Yang, X. Zheng, Z.-X. Jiang, X. Zhou, *J. Org. Chem.* 2015, **80**, 4443; d) Q. Peng, Y. Li, S. Bo, Y. Yuan, Z. Yang, S. Chen, X. Zhou, Z.-X. Jiang, *Chem. Commun.* 2018, **54**, 6000; e) C. Zhang, S. S. Moonshi, W. Wang, H. T. Ta, Y. Han, F. Y. Han, H. Peng, P. Král, B. E. Rolfe, J. J. Gooding, *ACS Nano* 2018, **12**, 9162; f) H. Zhang, Y. Li, S. Chen, Y. Yuan, Z.-X. Jiang, X. Zhou, *ACS Appl. Bio Mater.* 2019, **2**, 27.
- a) M. Ethirajan, Y. Chen, P. Joshi, R. K. Pandey, *Chem. Soc. Rev.* 2011, **40**, 340; b) X. Xue, A. Lindstrom, Y. Li, *Bioconjugate Chem.* 2019, **30**, 1585.
- a) S. Svenson, D. A. Tomalia, *Adv. Drug Delivery Rev.* 2005, **57**, 2106; b) E. R. Gillies, J. M. J. Fréchet, *Drug Discovery Today* 2005, **10**, 35; c) R. Duncan, *Nat Rev Cancer* 2006, **6**, 688; d) Y. Geng, P. Dalhaimer, S. Cai, R. Tsai, M. Tewari, T. Minko, D. E. Discher, *Nat Nanotechnol.* 2007, **2**, 249; e) A. R. Menjoge, R. M. Kannan, D. A. Tomalia, *Drug Discovery Today* 2010, **15**, 171.

## Journal Name

## ARTICLE

- 9 a) M. B. Taraban, Y. Li, F. Yue, E. V. Jouravleva, M. A. Anisimov, Z.-X. Jiang, Y. B. Yu, *RSC Adv.* 2014, **4**, 54565; b) M. B. Taraban, D. J. Deredge, M. E. Smith, K. T. Briggs, Y. Feng, Y. Li, Z.-X. Jiang, P. L. Wintrobe, Y. B. Yu, *RSC Adv.* 2019, **9**, 1956.

View Article Online  
DOI: 10.1039/D0TB00083C